

# Electronic structure and oxygen bonding in $\text{CaSiO}_3$ silicate

Nan Jiang<sup>1</sup>, J D Denlinger<sup>2</sup> and John C H Spence<sup>1</sup>

<sup>1</sup> Department of Physics and Astronomy, Arizona State University, Tempe, AZ 85287-1504, USA

<sup>2</sup> Advanced Light Source, Lawrence Berkeley National Laboratory, Berkeley, CA 94720, USA

E-mail: nan.jiang@asu.edu

Received 5 May 2003, in final form 7 July 2003

Published 1 August 2003

Online at [stacks.iop.org/JPhysCM/15/5523](http://stacks.iop.org/JPhysCM/15/5523)

## Abstract

Bonding of the bridging oxygen (BO) and non-bridging oxygen (NBO) sites in the  $\text{CaSiO}_3$  silicate is studied using soft x-ray emission, absorption and electron energy-loss spectroscopy of the oxygen K edge. Comparisons with APW + *lo* calculations are discussed, showing that this method can be applied successfully to silicates, which have large unit cells. Several specific features due to BO and NBO atoms in the density of states are reproduced by the calculations. The bonding in  $\text{CaSiO}_3$  is also examined using electron density maps. Our analysis of deformation electron density maps supports the idea that the NBO to Si bond is more ionic than the BO to Si bond.

## 1. Introduction

Silicates are of fundamental interest as glass and rock-forming materials. They are also widely used in ceramics, catalysts and electronic devices [1]. Other properties of silicates demonstrate their potential for new laser applications [2]. Recently, silicates have attracted much attention as alternative gate dielectrics in the semiconductor industry [3, 4]. The bonding characteristics of Si and O are essential in determining the properties of semiconductor devices, as well as the silicate glasses. However, the detailed nature of the Si–O bond remains a subject of discussion [5]. The theoretical and experimental studies of the electronic structure of silicates are thus needed for improved understanding of the properties of these materials. The electronic structure of a material is characterized by both the spatial and energy distribution of its electrons, which for crystals defines the band structure. Several spectroscopic methods have been used to measure band structure and the electron density of states (DOS). X-ray emission bands, for example, can provide information on the bonding of different atoms in silicates [6]. Detailed band structure calculations have also been carried out in several alkali silicates for comparison with experimental x-ray photoemission and photoelectron spectra [7].

The character of bonding in silicates can also be examined in terms of the ground-state electron density distribution, which can be measured using elastic scattering techniques, such

as x-ray and electron diffraction. Since excitation is avoided, only ground-state properties are probed. Electron density distributions have been measured in several silicates by x-ray diffraction [8, 9]. However, the poor diffraction quality of the samples causes problems of reproducibility [10]. Due to strong extinction effects, the results must be regarded as only qualitative [8]. Although quantitative electron diffraction overcomes the problem of extinction corrections [11], it has not been extended to systems with a large unit cell (e.g.  $>5 \times 5 \times 5 \text{ \AA}$ ). The theoretical modelling of the electron density distribution in silicates, however, is largely based on geometry-optimized molecules, such as  $\text{H}_6\text{Si}_2\text{O}_7$  [12]. Few studies in the literature have reported calculations on real crystal structures, probably because of the large unit cell and low degree of point symmetry in silicates [13, 14]. In this paper, we present calculations of the electron density distribution in  $\text{CaSiO}_3$ , based on the crystal structure of wollastonite-2M, using the augmented plane wave method, and comparisons with experimental spectra.

Our approach is to compare the calculated electron DOS in  $\text{CaSiO}_3$  with experimental measurements of soft x-ray emission (SXE), absorption (XAS) and electron energy loss spectra (EELS) to verify the calculations. The electron density distributions are then given in the form of difference charge-density maps, computed by subtracting a superposition of isolated neutral atom densities on  $\text{CaSiO}_3$  crystal sites from the electron density obtained from the calculations. The results are also discussed in comparison with experimental measurements from other silicates.

It is known that the emission and absorption spectra of solids result from transitions from occupied energy levels or bands to inner shell vacancies and from inner shells to empty states, respectively. In the single-particle approximation, the expressions for the intensity of emission bands have analogous expressions for absorption spectra [15]. If it is assumed that the relevant matrix element is not dependent on wavevector  $k$  and energy  $E$ , then  $I(E) \propto D(E)$ , in which  $D(E)$  is the electron DOS. In other words, the combination of absorption and emission techniques can, in principle, obtain both the occupied and unoccupied DOS. The local site, and dipole selection, properties of SXE, XAS and EELS provide the local DOS projected onto different atomic sites. This local assumption can be justified on the basis that the inner shell wavefunctions are sharply localized in the atom core region. Neglect of the matrix element variation, however, always causes discrepancies in comparisons between experimental spectra and calculations. Additionally, core-hole interactions must be considered. According to the final-state rule, applicable to metals at least, emission and absorption spectra can be simulated rather accurately from one-electron calculations, using wavefunctions obtained from the one-electron potential of the final state, i.e. including the core hole for absorption and excluding it for emission spectra [16]. In this work, all spectra (both emission and absorption) are compared with ground-state DOS calculations, so that core-hole effects in XAS and EELS are ignored. We expect that the core-hole interaction should produce strong effects on both Ca and Si absorption and EELS spectra but weak on O. This is because the core-hole interaction may be partially screened by the relatively high electron density around O atoms. In a recent work, we found that a simulation with half a core hole provides the best approximation to the final states on the B K edge in  $\text{MgB}_2$ , but a full core hole may overestimate the core-hole effects [17]. Therefore, only spectra of O are discussed in this work.

## 2. Theoretical calculations

### 2.1. Crystal structure

At room temperature,  $\text{CaSiO}_3$  has a chain silicate structure, with three  $[\text{SiO}_4]$  tetrahedra in the repeat unit. A series of polymorphs exist with different packing arrangements of the

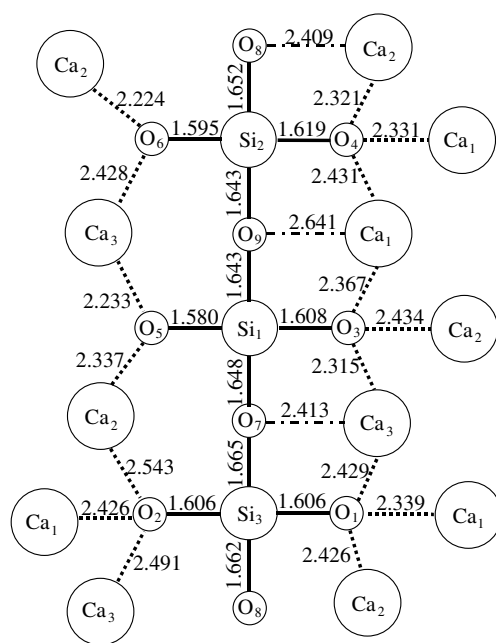


**Figure 1.** Schematic drawing of the bonding of the Si tetrahedral chain in wollastonite-2M  $\text{CaSiO}_3$ .

single chains [18]. The monoclinic phase, wollastonite-2M (parawollastonite), is related to the triclinic, wollastonite-1T, by a simple stacking modification. The unit cell of monoclinic wollastonite-2M contains 60 atoms, 15 of them at inequivalent sites. The space group is  $P2_1/a$ . The structure was refined by Hesse [19] and his lattice parameters ( $a = 15.409 \text{ \AA}$ ,  $b = 7.322 \text{ \AA}$ ,  $c = 7.063 \text{ \AA}$ ,  $\beta = 95.30^\circ$ ) and atomic coordination are used in our calculations. Figure 1 displays schematically the nearest-neighbour bonding structures of the inequivalent Si and O atoms. The Si tetrahedra are connected by  $\text{O}_7$ ,  $\text{O}_8$  and  $\text{O}_9$ , which are defined as bridging oxygen (BO). Other oxygen atoms, from  $\text{O}_1$  to  $\text{O}_6$ , only bond to one Si; therefore they are defined as non-bridging oxygen (NBO). Some of the NBOs have three nearest-neighbour Ca, while others ( $\text{O}_5$  and  $\text{O}_6$ ) only have two. It should be noted that all the BOs also bond with one nearest-neighbour Ca. In fact, the distances  $d_{\text{O}_7-\text{Ca}_3}$  and  $d_{\text{O}_8-\text{Ca}_2}$  are just about 1% longer than the corresponding average O–Ca bond lengths, but  $d_{\text{O}_9-\text{Ca}_1}$  is about 9% longer. The three Si tetrahedra are generally the same, with average Si–O distances (O–Si–O angle) of  $1.620 \text{ \AA}$  ( $109.2^\circ$ ),  $1.627 \text{ \AA}$  ( $109.3^\circ$ ) and  $1.635 \text{ \AA}$  ( $109.2^\circ$ ), respectively. It is noted that the average Si– $\text{O}_{\text{BO}}$  distance ( $1.652 \text{ \AA}$ ) is longer than that of the Si– $\text{O}_{\text{NBO}}$  ( $1.602 \text{ \AA}$ ). Three Ca atoms are approximately octahedrally coordinated with oxygen, with average Ca–O bond lengths of  $2.365$ ,  $2.378$  and  $2.385 \text{ \AA}$ , respectively.

## 2.2. Calculation of the density of states

Many methods have been developed for the calculation of electronic structure. One of the most commonly used is the full potential linearized augmented plane wave approach [20], which is a density-functional-based [21] electronic structure method, which refines the electron density iteratively by solving the Kohn–Sham equations [22] and the charge density alternately. The basis set consists of muffin-tin orbitals; inside the non-overlapping muffin-tin spheres the basis

functions are linear combinations of radial functions and their energy derivatives, while outside the spheres are plane waves [23]. The basis functions and their first derivatives are continuous at the muffin-tin spheres.

In this study, the band structure and deformation charge–density maps of  $\text{CaSiO}_3$  were calculated using the WIEN2K code [24], which is based on the augmented plane wave plus local orbital (APW + lo) method [25]. As an extension of the linearized augmented plane wave method, APW + lo uses a Slater standard augmented plane wave basis, and then adds a new local orbital (lo), which is zero at the sphere boundary, and normalized. The advantage of the APW + lo is that it converges to practically identical results as the linearized augmented plane wave method, but much faster. The Coulomb potential is expanded in the form of  $\sum_{lm} V_{lm}(r)Y_{lm}(\hat{r})$  within MT and  $\sum_K V_K e^{iK \cdot r}$  outside the muffin-tin, which is solved based on the concept of multipole potentials and the boundary value problem for a sphere [26]. For the exchange–correlation potential, the generalized gradient approximation is employed [27]. The total energy is thus computed according to Weinert *et al* [28]. In our calculations, the radii of the muffin-tin spheres are  $R_{\text{MT}} = 2.0, 1.5$  and  $1.48$  au for Ca, Si and O atoms, respectively, with a cut-off  $RK_{\text{max}} = 7.0$ . Since the unit cell of  $\text{CaSiO}_3$  is large, only 500  $k$  points in the irreducible zone were calculated to save computing time. The differences between calculating 500 and 5000  $k$  points, for example in quartz ( $\text{SiO}_2$ ), are insignificant; the van-Hove-type peaks become smoother with increasing  $k$  points in the calculations. Nevertheless, the sharp van-Hove-type peaks, in general, are too detailed to be observed in our experimental spectra, due to broadening from final-state lifetimes and instrument resolution.

### 3. Experiment

Crystalline samples were prepared by annealing glassy  $\text{CaSiO}_3$  at  $1000^\circ\text{C}$  for 2 h. Samples were kindly supplied by Dr Qiu of Shanghai Institute of Optics and Fine Mechanics. The x-ray intensities of the powder samples match those of standard wollastonite-2M. Electron microscope specimens were prepared by picking up tiny pieces of crystals suspended in acetone on a lacy carbon film spanning a copper grid. The specimens were observed in a Philips EM400 with a field-emission gun and a Gatan parallel EELS system. The energy resolution of the spectrometer is about 1.0 eV. Backgrounds were fitted at pre-edge intensities using a power-law form and subtracted from the original data.

SXE and XAS experiments were performed at the ALS Beamline 8.0 using the Tennessee/Tulane grating spectrometer with experimental emission and absorption spectral resolutions of  $\sim 0.3$  and  $\sim 0.1$  eV, respectively. SXE, measured with a  $1500 \text{ lines mm}^{-1}$  grating spectrometer for fixed photon energy excitation above the O K-edge threshold, is used as a probe of the dipole-selective occupied valence band partial DOS, i.e. oxygen p states. XAS, a probe of unoccupied conduction band states, was measured by partial fluorescence yield with the detection window covering the entire emission. The absolute XAS photon energies were calibrated using a  $\text{TiO}_2$  [29].

## 4. Results and discussion

### 4.1. Density of states

Figure 2 compares the calculations of the occupied and unoccupied O p DOS in  $\text{CaSiO}_3$  with emission bands (SXE) and absorption spectra (XAS and EELS). The relative energy calibration between SXE and XAS was determined by the presence of weak elastic scattering in SXE spectra, and thus indicates a  $>5$  eV bandgap in  $\text{CaSiO}_3$ . Two distinct excitation

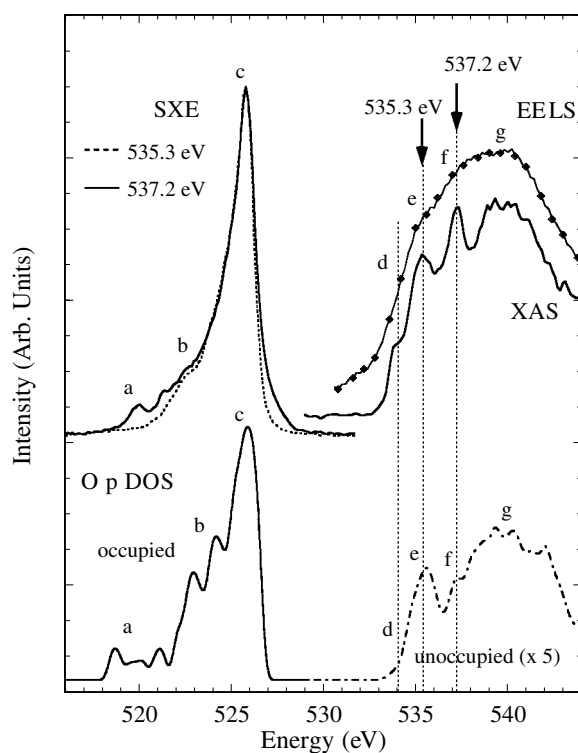


**Figure 2.** Comparison of experimental O K SXE, XAS and EELS with calculated O 2p DOS. The DOS has been broadened to 0.5 eV using Gaussian function.

energies of the O K emission spectra are identified in the absorption spectrum (indicated by arrows in figure 2); they are 535.3 and 537.2 eV, respectively. In SXE spectra, there is a major peak (marked as (c)) with several 'satellite' features (marked as (a) and (b)) on the low-energy side. The differences between the two spectra are obvious. At lower excitation energy, peak (a) disappears in the spectrum and peak (b) is also weaker than that at the higher excitation energy. The SXE spectra at other energies have also been observed. The spectra near the threshold energy are similar to those recorded at 535.3 eV, while those at energies higher than 537.2 eV are similar to those recorded at 537.2 eV. The occupied O p DOS is aligned to the highest peak (c) of the O K emission band and the corresponding features in the O p DOS are also indicated. It is seen that the overall features are similar in the calculated O p DOS and measured O K SXE, although there are some differences in details. The bandwidth of the O K emission is about 9–10 eV, which is close to the 9.0 eV (after 0.5 eV broadening) of the calculations. However, peak (c) in the SXE spectra is narrower and the relative intensity of peak (b) is much weaker than that in the O p DOS. Additionally, peak (a) in the calculations is not a single peak, as in the experiment.

The overall shape of the O K-edge XAS and EELS spectra are similar to each other, although the EELS spectrum is broader than the XAS because of the lower energy resolution in the EELS spectrometer. Four common features can be recognized in each spectrum, marked (d), (e), (f) and (g), respectively. These features are qualitatively consistent with the calculations of the unoccupied O p DOS, in which the corresponding features are also indicated, despite the neglect of final-state effects. Both the EELS spectrum and the unoccupied O p DOS are

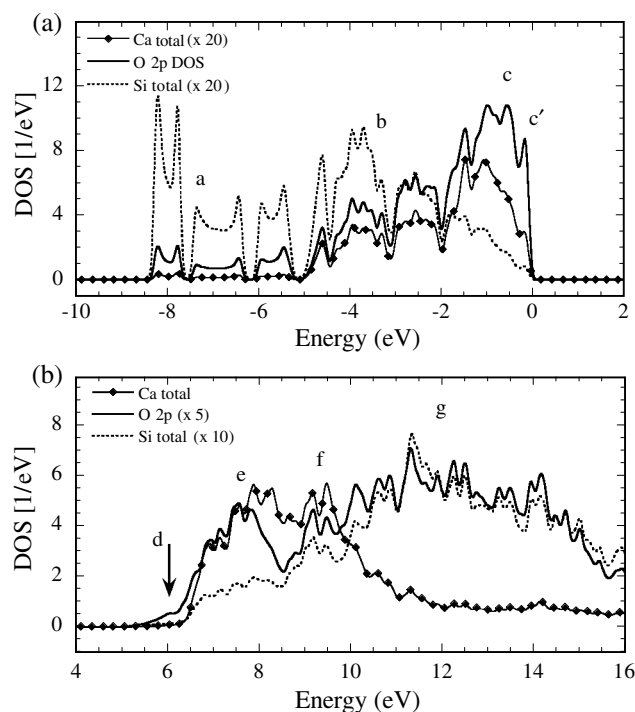


**Figure 3.** Comparison of (a) occupied and (b) unoccupied O 2p DOS with Ca and Si total DOS.

aligned to the threshold of the XAS spectrum. However, there are significant discrepancies in the relative intensities of peaks (d) and (f). The threshold of the absorption spectrum is a profound peak (d), but it is only a tail-like feature in the calculations. In the experiment, peak (f) is also very strong and sharp, but it is very weak in the calculations.

We note that the O K emission band of  $\text{CaSiO}_3$  is very similar to that of other silicates [30]. In terms of molecular orbital theory, peak (a) can be assigned to the interactions between O and Si orbitals, peak (b) comes from O orbitals mixed with both Si and Ca, while peak (c) is dominated by the interaction between the O and Ca orbitals. These assignments can be justified by comparisons with band structure calculations. The O 2p DOS are compared with the Si and Ca LDOS in figure 3(a). The letters indicate the locations of the features in O K emission corresponding to figure 2. It is seen that Ca makes no contribution to the O 2p band in the low-energy region ( $-8.5$  to  $-5$  eV). In the middle ( $-5$  to  $-3$  eV), both Si and Ca have contributions, but the Si features are stronger than the Ca. In the high-energy region ( $> -2$  eV), Ca characteristics dominate. It is also found that the top of the O 2p band (marked as (c)') is purely O in character. In other words, the band edge is determined by the O 2p non-bonding states.

It should be noted that the lower part (between 6.5 and 16 eV) of unoccupied states is profoundly dominated by the Ca characteristic. In this region, the Si features increase with increasing energy, although they are less dominant than the Ca (figure 3(b)). In the higher energy region ( $> 16$  eV), on the contrary, the Si features are much stronger than the Ca (not showing in figure 3(b)). Interestingly, the lowest states of the conduction band are purely O characteristic, although the intensity is small. Therefore it is reasonable to conclude that

peak (d) is the O 2p non-bonding states. Peak (e) is dominated by the O–Ca interaction, with less contribution from the Si. Although peak (f) is still dominated by the O–Ca interactions, the contribution from the O–Si interactions also increases. Peak (g) can be considered to be the mixture of the O–Ca and O–Si interactions, in which both Si and Ca DOS have the same magnitude.

The above assignments of the features in the experimental spectra to the calculated DOS are only qualitative. The intensities and widths of some features are not quantitatively consistent between experiments and calculations. In the O K emission band, peak (a) is a single-peak-like feature, but it is much wider in the calculations, and the relative intensity of feature (b) is much less than that in the calculations. Most importantly, peak (c) is much narrower in experiments than in calculations. The discrepancy may result from calculations due to the complicated crystal structure of  $\text{CaSiO}_3$ . As mentioned above, oxygen has nine inequivalent sites in the wollastonite-2M unit cell of  $\text{CaSiO}_3$ , which may be approximately divided into BO and NBO types (see figure 1). Although the environments of BO and NBO are similar within the group, differences exist in the bonding lengths and angles. These result in the calculated O p DOS projected onto inequivalent sites, within the BO and NBO groups, respectively, being slightly different from each other, although their overall shapes are similar. The O p DOS projected onto nine inequivalent sites are plotted in figure 4. It is seen that the valence states of the O p DOS on  $\text{O}_2$ ,  $\text{O}_4$  and  $\text{O}_6$ , for example, are slightly different. The major difference is that the O non-bonding peak (marked as (c)') at the top of the valence band is absent in the p DOS on  $\text{O}_1$ , exists on  $\text{O}_3$ , but becomes very strong on  $\text{O}_6$ . As a result, the broad peak (c) of the total O p DOS in figure 2 consists of both O–Ca and O–O interactions. In other words, the O–O interactions have less contribution in the experimental spectra than the theoretical prediction. The reason for this is unclear. Additionally, the calculations are using the experimental data for the geometry, without relaxation of atomic positions. Therefore, it is not the real ground state of the system, although it is close to it.

In the  $\text{CaSiO}_3$ , there are three inequivalent Si and Ca sites, respectively, but they have similar local structures. The overall local DOS on the different Si and Ca are similar, although differences exist in their fine structures. However, they are not discussed in this study.

Another important feature in figure 4 is that the occupied O p DOS on the BOs are more dispersive than those on the NBOs. The O p DOS on the BO and NBO sites are compared in figure 5. (The magnitude of the unoccupied DOS has been increased by a factor of 5.) It is seen that the O p DOS on NBO is from  $-5.0$  to  $0$  eV, but it is from  $-8.5$  to  $0$  eV for BO. The band centres for NBO and BO are at about  $-1.8$  and  $-3.5$  eV, respectively. As a result, peak (a) in the O K emission band (figure 2) can also be considered to be characteristic of BO, or the Si–O–Si interactions. Therefore, it is reasonable to conclude that the O K emission band obtained at the excitation energy of  $535.3$  eV has little contribution from BO. In contrast, at the excitation energy of  $537.2$  eV, BO as well as NBO has significant contribution.

In principle, the site selection of x-ray emission is based on the fact that the possibility of transitions from a valence electron localized on one atom to a vacancy on a neighbouring atom is small [31]. Therefore, tuning the excitation energy to promote a core electron to an unoccupied state, which is strongly localized on a particular site, can separate the SXE spectra from identical atomic species with different bonding characteristics [32]. Even if the unoccupied states, localized on different sites, overlap it is still possible to obtain site selectivity, by identifying excitation energies for which one particular site makes the dominant contribution.

According to the site selection of SXE spectra, the unoccupied O 2p states at energies of  $535.3$  and  $537.2$  eV are dominated by the NBO and BO, respectively. As shown in figure 5, the calculations show that the unoccupied O p DOS on both BO and NBO are significantly

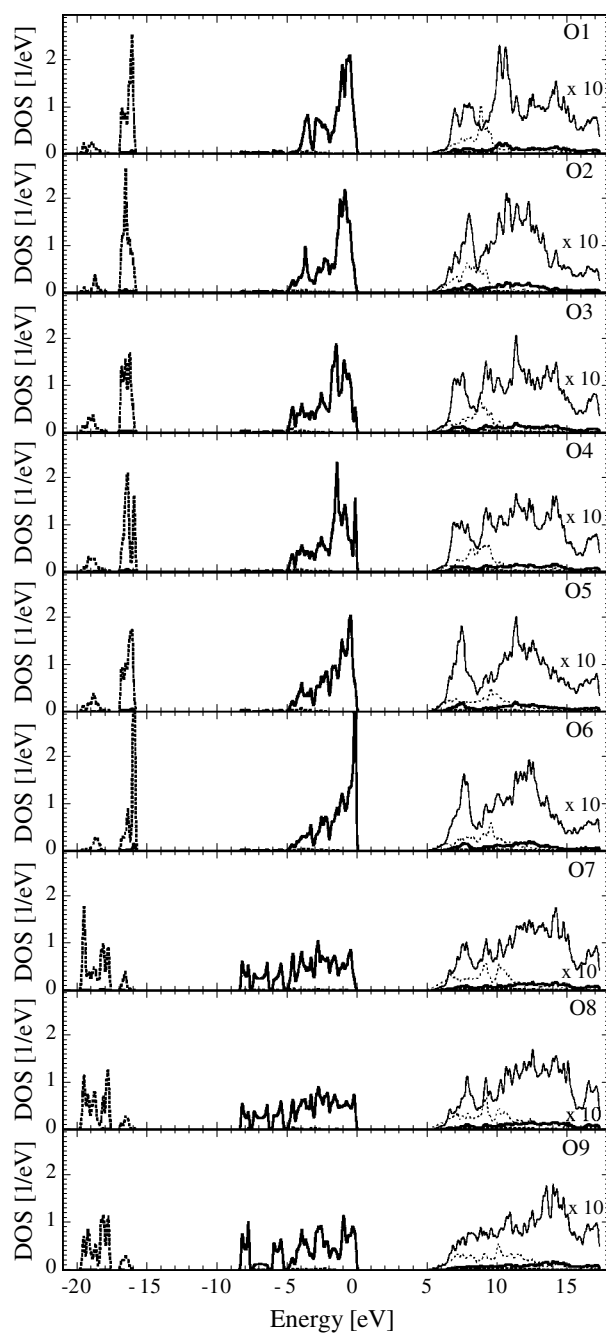


**Figure 4.** O 2p DOS projected on inequivalent sites.

different from each other. On NBO it has a relatively high intensity at the bottom of the unoccupied states, while on BO it shows an increasing trend with increasing energy to about 14 eV. This is consistent with a previous study in a Ca aluminosilicate system [33]. Although the calculations do not clearly show a sharp absorption peak at 537.2 eV, the relative intensity

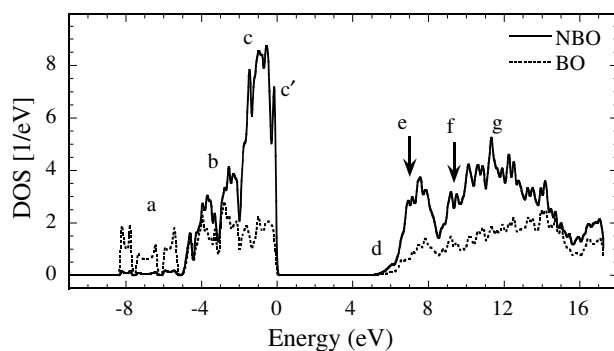


**Figure 5.** Comparison of O 2p DOS between BO and NBO.

of O p DOS on BO in this peak is higher than that in the peak at 535.3 eV. Therefore, tuning the excitation energy to 535.3 and 537.3 eV will significantly increase the possibilities of the emission from NBO and BO, respectively. This is consistent with the assignments of observed features in the emission band. The interactions between Si and BO are stronger than that between the Si and NBO, and thus features (a) and (b) are stronger when the excitation energy is tuned to 535.3 eV.

#### 4.2. Deformation density maps

Deformation density is defined as the difference between the total electron density for the crystal and the density calculated using a reference model. In this work, the reference consists of a superposition of spherical ground-state atoms. Figure 6 shows two deformation density maps around O and Si. Figure 6(a) shows that electron density is highly concentrated along the chains of Si tetrahedra, which are linked by shared oxygen atoms at corners (BO). There are deep and shallow negative valleys of density between the two oxygen and two silicon atoms, respectively. This indicates localization of electrons around the oxygen atoms. The electron density maxima  $\sim 0.24 \text{ e } \text{\AA}^{-3}$  in height are displaced towards the more electronegative O atoms, at a distance of  $\sim 40\%$  of the O–Si bond length from O, and away from the Si–O line into the interior of the Si–O–Si angle. The latter phenomenon has been associated with Si–Si static repulsion [34]. We also note that there are bridges of density across the interior of the bent Si–O–Si angles and well-defined sharp non-bonding peaks close to oxygen on the external side of the bend. Experimentally, non-bonding deformations behind the O atom have also been observed in two other chain silicates: CaMgSi<sub>2</sub>O<sub>6</sub> and LiAlSi<sub>2</sub>O<sub>6</sub> [35]. All these features have been noted in calculations of molecular H<sub>6</sub>Si<sub>2</sub>O<sub>7</sub> [5]. This is reasonable because molecular H<sub>6</sub>Si<sub>2</sub>O<sub>7</sub> can be considered as the simplest model for the edge-shared Si tetrahedral chain.

Figure 6(b) gives the deformation density map on a BO and on a NBO plane. The differences between BO and NBO are noted: the electron density maxima is about  $0.03 \text{ e } \text{\AA}^{-3}$  higher on the NBO–Si bond and displaced by about 3% of the Si–O bond length toward NBO. In other words, the ionicity of the NBO–Si bond is stronger than that of the BO–Si bond. This conclusion is consistent with other calculations [36]. The maxima are situated just on the bond line, which is different from the BO–Si bond in figure 6(a). We also note that there are two well-defined non-bonding peaks close to the NBO behind the O–Si bond.

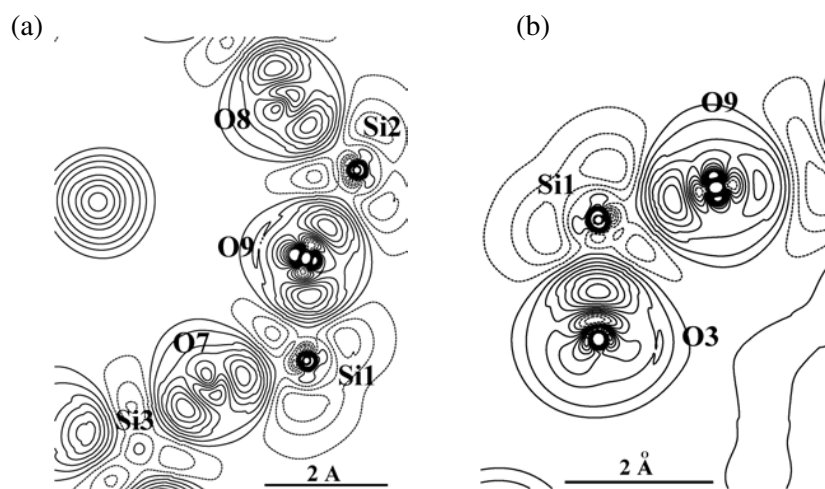


**Figure 6.** Electron deformation density map showing bonding characteristics along the Si tetrahedral chain in (a) and the difference between BO and NBO in (b).

## 5. Conclusions

In this paper, we have shown that the APW + *lo* method can be applied successfully to silicates, which have large unit cells. The calculations for  $\text{CaSiO}_3$  can properly interpret experimental x-ray emission, absorption and EELS spectra. Several specific features due to BO and NBO in the DOS are reproduced by the calculations. Bonding in  $\text{CaSiO}_3$  has also been examined using electron density maps. Our analysis of deformation electron density maps supports the idea that the NBO to Si bond is more ionic than the BO to Si bond. It is also noted that small discrepancies remaining between calculations and experiments could perhaps come from the non-relaxed calculation.

## Acknowledgments

This work was supported by NSF award DMR0245702. We thank Dr J Qiu of Shanghai of Optics and Fine Mechanics for supplying the  $\text{CaSiO}_3$  crystals, Dr T Groy of Arizona State University for assistance and Dr B Jiang for a discussion of deformation densities.

## References

- [1] See, for example, Lackner K S, Wendt C H, Butt D P, Joyce E L and Sharp D H 1995 *Energy* **20** 1153
- [2] Avanesov A G, Lebedev V A, Zhorin V V, Okhrimchuk A G and Shestakov A V 1997 *J. Lumin.* **72–74** 155
- [3] Lucovsky G, Rayner G B, Kang D, Appel G, Johnson R S, Zhang Y, Sayers D E, Ade H and Whitten J L 2001 *Appl. Phys. Lett.* **79** 1775
- [4] Jameson J R, Harrison W and Griffin P B 2001 *J. Appl. Phys.* **90** 4570
- [5] Gibbs G V, Downs J W and Boisen M B Jr 1994 *Rev. Mineral.* **29** 331 and references therein
- [6] Urch D S 1989 *Mineral. Mag.* **53** 153 and references therein
- [7] Ching W Y, Murry R A, Lam D J and Veal B W 1983 *Phys. Rev. B* **28** 4724  
Ching W Y, Li Y P, Veal B W and Lam D J 1985 *Phys. Rev. B* **32** 1203
- [8] Tsirelson V G, Evdokimova O A, Belokoneva E L and Urusov V S 1990 *Phys. Chem. Miner.* **17** 275 and references therein
- [9] Sawada H 1999 *J. Solid State Chem.* **142** 273

- [10] Van der Wal R I, Vos A and Kirfel A 1987 *Acta Crystallogr. B* **43** 132
- [11] Zuo J, Kim M, O'Keeffe M and Spence J C H 1999 *Nature* **401** 49
- [12] Gibbs G V, Hill F C and Boisen M B Jr 1997 *Phys. Chem. Miner.* **24** 167 and references therein
- [13] D'Arco Ph, Fava F F, Dovesi R and Saunders V S 1996 *J. Phys.: Condens. Matter* **8** 8815
- [14] Munakata K and Yokoyama Y 2001 *J. Nucl. Sci. Technol.* **38** 915
- [15] Meisel A, Leonhardt G and Szargan R 1989 *X-ray Spectra and Chemical Binding (Springer Series in Chemical Physics vol 37)* (Berlin: Springer)
- [16] von Barth U and Grossmann C 1980 *Phys. Scr.* **21** 580
- [17] Jiang B, Jiang N and Spence J C H 2003 *J. Phys.: Condens. Matter* **15** 1299
- [18] Wenk H-R 1969 *Contrib. Min. Petr.* **22** 238
- [19] Hesse K-F 1984 *Z. Kristallogr.* **168** 93
- [20] For a review see, Singh D 1994 *Planewaves, Pseudopotentials, and the LAPW Method* (Boston, MA: Kluwer-Academic)
- [21] Hohenberg H and Kohn W 1964 *Phys. Rev. B* **136** 864
- [22] Kohn W and Sham L J 1965 *Phys. Rev. A* **140** 1133
- [23] Anderson O K 1975 *Phys. Rev. B* **12** 3060
- [24] Blaha P, Schwarz K, Madsen G K H, Kvasnicka D and Luitz J 2001 *WIEN2K, An Augmented Plane Wave+Local Orbitals Program for Calculating Crystal Properties* ed K Schwarz (Austria: Tech. Universität Wien) ISBN 3-9501031-1-2
- [25] Sjöstedt E, Nordström L and Singh D J 2000 *Solid State Commun.* **114** 15
- [26] Weinert M 1981 *J. Math. Phys.* **22** 2433
- [27] Perdew J P, Burke S and Ernzerhof M 1996 *Phys. Rev. Lett.* **77** 3865
- [28] Weinert M, Wimmer E and Freeman A J 1982 *Phys. Rev. B* **26** 4571
- [29] Lusvardi V S, Barteau M A, Chen J G, Eng J Jr, Fruhberger B and Teplyakov A 1998 *Surf. Sci.* **397** 237
- [30] AlKadier M A, Tolon C and Urch D S 1984 *J. Chem. Soc. Faraday Trans. II* **80** 669
- [31] Watson L M 1973 *Band Structure Spectroscopy of Metals and Alloys* ed D J Fabian and L M Watson (London: Academic) p 125
- [32] Nordgren J and Wassdahl N 1995 *J. Electron Spectrosc. Relat. Phenom.* **72** 273 and references therein
- [33] Jiang N 2002 *Solid State Commun.* **122** 7
- [34] O'Keeffe M and Gibbs G V 1985 *J. Phys. Chem.* **89** 4574
- [35] Sasaki S, Fujino K, Takeuchi Y and Sadanaga R 1980 *Acta Crystallogr. A* **36** 904
- [36] Kowada Y, Adachi H, Tatsumisago M and Minami T 1994 *J. Non-Cryst. Solids* **177** 286